Pergamon

0148-9062(93)E0007-B

Int. J. Rock Mech. Min. Sci. & Geomech. Abstr. Vol. 31, No. 4, pp. 323–345, 1994
Copyright © 1994 Elsevier Science Ltd
Printed in Great Britain. All rights reserved
0148-9062/94 $7.00 + 0.00

Rock Mechanics Investigations for Rock Slope Stability Assessment

P. LUNARDI†
P. FROLDI‡
E. FORNARI§

This paper describes investigations, geophysical and geomechanical studies of rock masses, carried out in order to analyse the stability of excavations for the Ravedis Dam and the slopes of the catchment basin upstream from the dam. A thorough geostructural survey revealed a network of discontinuities that characterizes the rock masses. Seismic tomographic investigations, analyses of data from raise borer drillings and in situ shear tests on blocks of rock were carried out in order to obtain a geomechanical picture of the density and strength of the rock masses. Geomechanical sections of the slopes were constructed by integrating geostructural, geophysical and geomechanical data; the stability of the slopes was analysed by using a slices equilibrium limit method, generally used in soil mechanics (Bell method). The computer program employed with this method was modified to take into account non-linear strength characteristics, according to the Hoek and Brown criterion, and also the possibility that failure surfaces may develop along natural discontinuities.

Reinforcement of the rock mass with an artificial increment in cohesion was simulated using the concept of "reinforced rock".

INTRODUCTION

Large excavation works of rock surfaces for civil engineering projects and mining activities mean that the stability of the excavations must be studied and a numerical safety coefficient calculated. In the particular case of excavations for the construction of a dam the safety of the slopes must be guaranteed for long periods of time and at least as long as the life of the dam itself.

In the case of the Ravedis Dam, two main problems of a geomechanical nature were identified:

1. calculation of the safety coefficient for the slopes affected by the excavation (more than 130 m in height), for the foundation of the dam and the excavation (more than 70 m in height), for the construction of the basins and for surface discharge (spillways). All excavations, except for those for the foundations of the dam, are to be considered as permanent works.
2. calculation of the safety coefficient for the natural slopes situated immediately upstream from the dam.

The authors used the Bell equilibrium limit method [1] for these calculations due to its ease of use and its reproducibility.

The method as modified by the authors will allow the following:

—the use of a non-linear failure criterion (Hoek and Brown);
—incorporation of discontinuities surfaces;
—inclusion of reinforcement operations using an artificial increment in cohesion.

The collection of information on the following was necessary for equilibrium limit stability analysis:

—principal structural elements (bedding, faults);
—joint network;
—degree of compactness (density) of the rock masses;
—shear strength of the rock masses.

This knowledge, quoted above, was obtained by means of the following investigations:

—aerial photogrammetric survey of the major tectonic structures;
—field survey of the major structures;
—field survey of the joint network;
—collection of data from raise borer drilling (hydraulic shafts);

†University of Parma, Parma, Italy.
‡Rocksoil Ltd, Milan, Italy.
§Zollet Engineering Ltd, S. Giustina, Belluno, Italy.

—tomographic surveys;
—*in situ* shear tests.

This paper gives a description of all the investigations and the design studies carried out including details of the modifications introduced to the computer program equations employed by the Bell method. This was done to take into account the strength criterion of Hoek and Brown, the existence of natural discontinuities and an increment in the strength properties resulting from reinforcement of the rock.

GEOGRAPHICAL AND GEOLOGICAL SETTING

The area where the Ravedis Dam is being constructed is situated in the piedmont transition belt between the Carnic PreAlps (Southern Alps) and the Venice–Friuli plane (Fig. 1). The geological formations outcropping on the surface consist of sedimentary reef facies (calcareous lithologies) and are affected by tectonic forces of a predominantly compressive kind.

The major structures are folds and thrusts with the axis running approximately NE–SW and the vergency S–SE. The principal plicate structures like that of Ravedis run along an ENE–WSW axis and are associated with faults crossing the axis of the folds at right angles to these (master faults, Fig. 2). The zone of the dam consists of an asymmetric overturned anticlinal fold (Fig. 3) with thrust at depth.

The present formation consists of carboniferous rocks of the Jurassic–Cretaceous period. The stratification of the calcareous sequence is generally regular with the thickness of the strata varying from a few centimeters to some meters. Clayey-silt intercalations of a plastic nature are present at times.

Due to the intense tectonization, the degree of fracturing of the material is very high and generally the spacing between discontinuities is measurable in centimetres.

STRUCTURAL SURVEY

The main structural element consists of an asymmetric overturned anticlinal fold, the axis of which runs NE–SW and develops along the valley (Fig. 2). The fold was studied by means of analysis of aerial photographs and field survey. It does not show large axial undulations and can be considered cylindrical. The strong folding has given rise to inter-strata slipping and faults at right angles to the development of the fold. Of note are some large structures running at right angles to the axis of the fold (master faults, Fig. 2: F6, F7, F8, F9, F10) and these lie in the zone of the site of the dam.

As the geostructural situation is very complex, the study was divided into two distinct stages.

I—survey for gathering of position data (dip and dip direction) concerning surface and underground (tunnel for bottom discharge and exploration pilot tunnels along the axis of the dam) discontinuities.
II—survey of position data and geomechanical characteristics of a few significant points (pilot surveys).

The following discontinuity data were obtained from the pilot surveys:

—dip and dip direction
—spacing
—consistency
—JCS (joint compressive strength)
—JRC (joint roughness coefficient)

The first stage of the survey involved 105 structural surveys providing 787 items of position data. The second stage of the survey consisted of 7 pilot surveys numbered R1, R2, R3, R6, R8, R9 and R10 providing 473 items of position data (Fig. 2). The average values for the geomechanical data collected in this stage are shown in Table 1. Altogether, 1260 items of structural data were collected; the stereographic projections (lower hemisphere of Schmidt) of the average discontinuities for the pilot surveys are given in Fig. 2.

The geostructural analysis resulted in the construction of a parallel, flexural, cylindrical type model of the fold (Fig. 3). The geometry of the fracturing systems showed the mechanism of the fold, similar to that of a curved slab, and its essential parts (Fig. 3):

—a decompressed external upper zone where the fracture network is the result of relaxed stress conditions: this is found on the right side of the valley;
—a compressed internal lower zone where the fractures network is caused by compressive conditions: this is found on the left side of the valley.

The two zones are in theory separated by a neutral centreline. The compact characteristics of the rock found *in situ* provided confirmation of the structural model.

RAISE BORING DATA PROCESSING

The Raise Boring technique (Fig. 4) was used for the excavation of the vertical access shafts to the sluice gate chambers and the descent passages (inclined shafts) for surface discharges (spillways). The machines used were of the Robbins 73 type with a diameter of $d = 2.13$ m and a 500 V motor.

After drilling of the pilot hole (dia. = 300 mm) during the ascent of the cutter, the following were measured:

—duration of each individual drilling phase (t) [min]
—velocity of advance (V_{av}) [m/hr]
—intensity of discontinuous current absorbed (I) [A]

The bore drilling resulted in the following:

right inclined shaft	40.5 m approx.
left inclined shaft	39 m approx.
right shaft	28.5 m approx.
left shaft	28.5 m approx.

A total of 136.5 m was drilled with this technique. The data obtained were processed to obtain a parameter for a qualitative evaluation of the compactness of the rock, the specific energy of the excavation (SE_v: energy consumed for the excavation of 1 m^3 of rock = specific

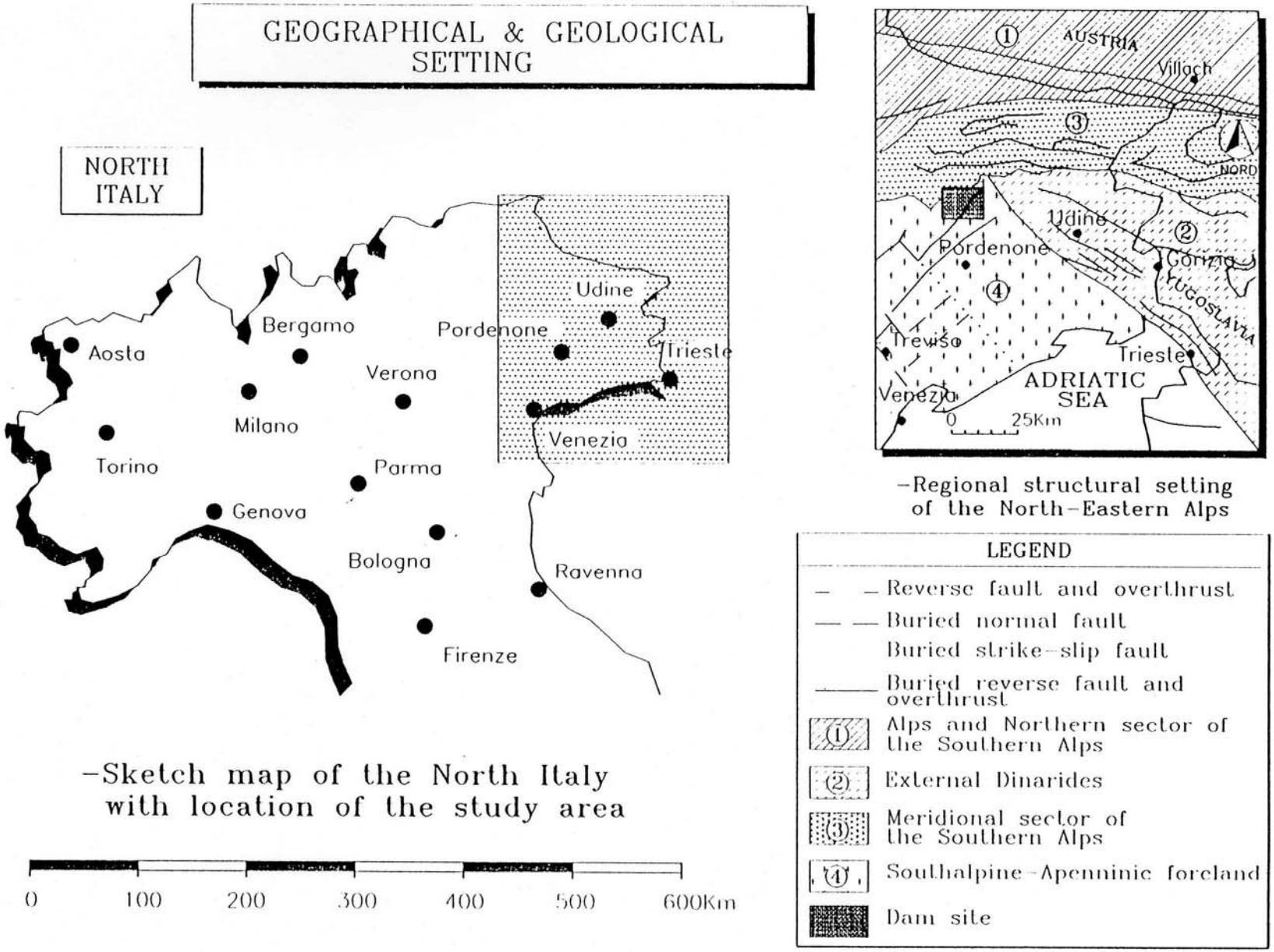

Fig. 1. Maps showing the geographical location of the study area in North Italy and the geological setting in the Eastern Alps.

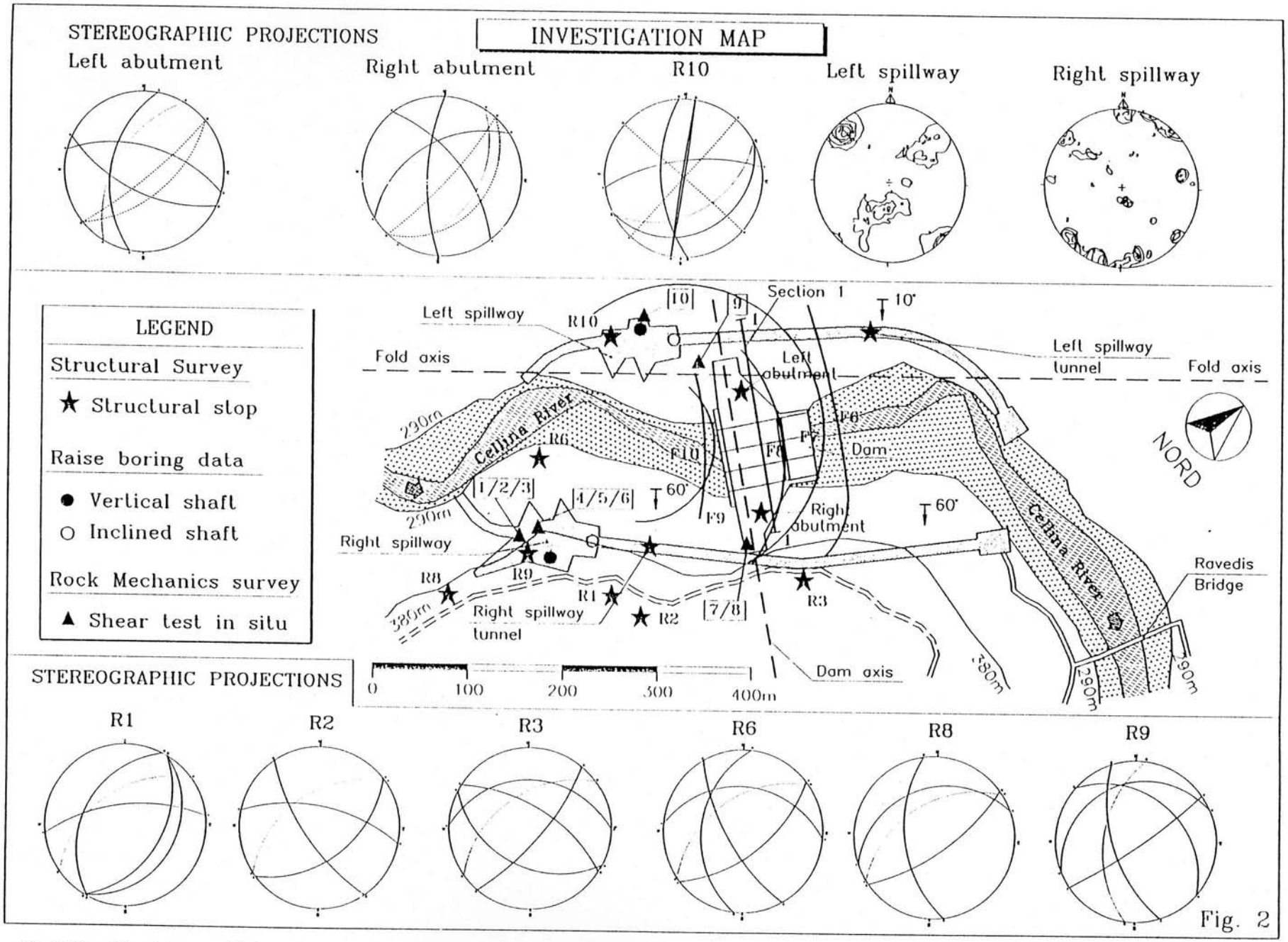

Fig. 2

Fig. 2. Map of the study area with the major tectonic features, the location of the structural survey, raise boring drilling and shear tests *in situ* and the stereographic projections of the collected joint data.

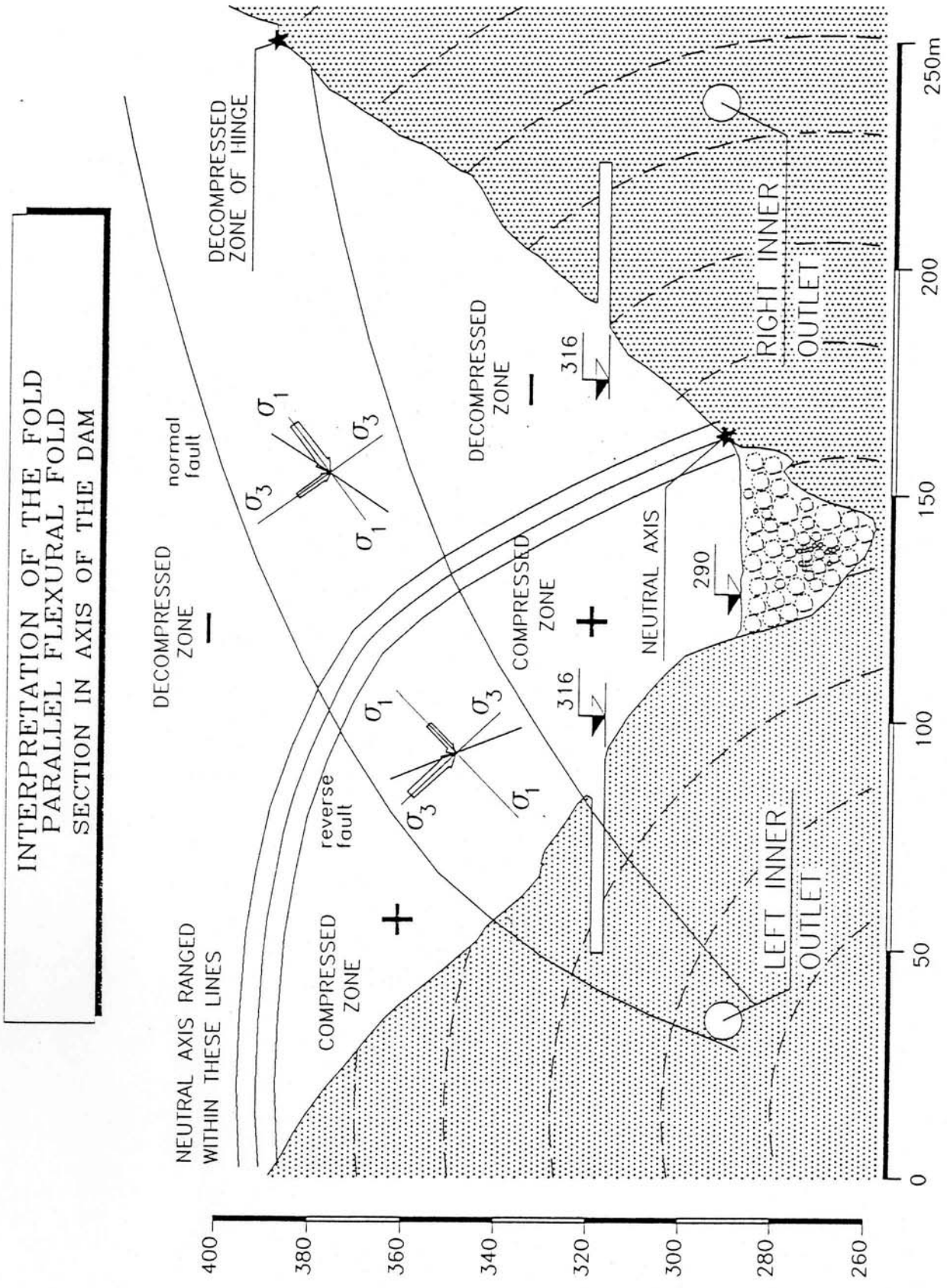

Fig. 3. Interpretation of the geometry of the fold by analysis of the structural patterns.

Table 1

Structural stop	Set	Joint type	Dip. direction	Dip.	Spacing (m)	Surface roughness	JRC	JCS (MPa)
R1	1	Bed	125°	50°	0.4	Smooth	8	50
	2	Fract.	300°	55°	0.3	Smooth	11	65
	3	Fract.	355°	75°	0.4	Flexuous	14	50
R2	1	Bed	145°	60°	0.1	Smooth	6	54
	2	Fract.	235°	80°	0.3	Smooth	8	50
	3	Fract.	15°	65°	0.1–0.5	Scabrous	10	40
R3	1	Bed	135°	80°	0.3–0.5	Scabrous	12	45
	2	Fract.	210°	60°	0.5–1.0	Flexuous	11	54
	3	Fract.	15°	40°	0.2–0.4	Scabrous	12	55
	4	Fract.	25°	65°	0.4–0.6	Scabrous	13	45
R6	1	Bed	145°	70°	0.4–1.0	Flexuous	6	47
	2	Fract.	240°	80°	0.3	Dentate	15	55
	3	Fract.	10°	45°	0.5–1.0	Scabrous	13	40
	4	Fract.	285°	50°	0.3	Scabrous	15	55
R8	1	Bed	145°	80°	0.6–1.5	Smooth	8	43
	2	Fract.	340°	35°	0.1–0.4	Smooth	9	51
	3	Fract.	260°	70°	0.1–0.5	Dentate	15	48
R9	1	Bed	145°	80°	0.1–0.2	Smooth	6	45
	2	Fract.	252°	58°	—	Flexuous	12	50
	3	Fract.	40°	30°	—	Scabrous	13	40
	4	Fract.	337°	17°	—	Flexuous	12	50
R10	1	Bed	150°	20°	—	Smooth	2	30
	2	Fract.	350°	65°	—	Flexuous	12	30
	3	Fract.	100°	90°	—	Dentate	12	30
	4	Fract.	265°	60°	—	Flexuous	12	30

energy (volumetric) [kWh/m³]. Processing of the data involved subjecting it to the following procedure (the symbols used are those already given):

$$SE_v = \frac{V \cdot I}{d^2 \cdot V_{av}} \cdot 1249[\text{kWh/m}^3]. \quad (1)$$

The number 1249 derives from homogenization of the units of measurement. Statistical processing of the precise data for each single drilling phase produced the results given in Table 2. The results of the processing of the data led to various observations.

The specific energy employed was greater during the advance of the pilot hole where the drilling took place in a mass not yet stress relaxed and on a scale affected by few structural discontinuities. No significant differences were encountered between the left and the right shafts. On the other hand, the specific energy was very low during the widening phase with the Raise Borer, where drilling took place in a mass that was already stress relaxed by the drilling of the pilot hole and that involved numerous structural discontinuities. The difference between the values found for the left side (compacted mass) compared to those for the right (stress relaxed mass) was significant.

The specific energy values that emerged from the data processing have been expressed in a graph as a function of depth from the topographical surface (Figs 5, 6, 7 and 8).

Examination of the graphs shows that:

—the linear interpolations on the graphs for the descent passages (inclined shafts) show considerable variation with depth;

—the linear interpolations carried out on the graphs for the vertical shafts show an almost constant trend;

—on the right side, a decrease in SE_v occurs towards the surface where the relaxation of the slope contributes to an increase in the ease with which the rock mass was drilled;

—on the left side a decrease in SE_v is seen at a depth where the greater ease with which the rock mass was drilled can be put down to greater tectonization of the rock in the heart of the fold.

For a calculation of a quantitative index defining the ratio (R) between specific energy used on the left side as compared to that used on the right side, the integral of the linear interpolation line on all the graphs was developed.

R is defined as R = ratio between specific energies integrated over the length of the drilling, where:

$$\int_{z1}^{z2} SE_v[\text{kWh/m}^3]dz = SE_a[\text{kWh/m}^2]$$

$$= \text{integrated specific energy} \quad (2)$$

where

SE_v = specific energy for unit of volume
SE_a = specific energy for unit of surface.

The ratio R assumes the following values:

R vs (vertical shafts) = 1.32
R is (inclined shafts) = 1.39.

Both ratios are greater than one and confirm the greater overall compactness of the left side with respect to the right side as shown in the geostructural model.

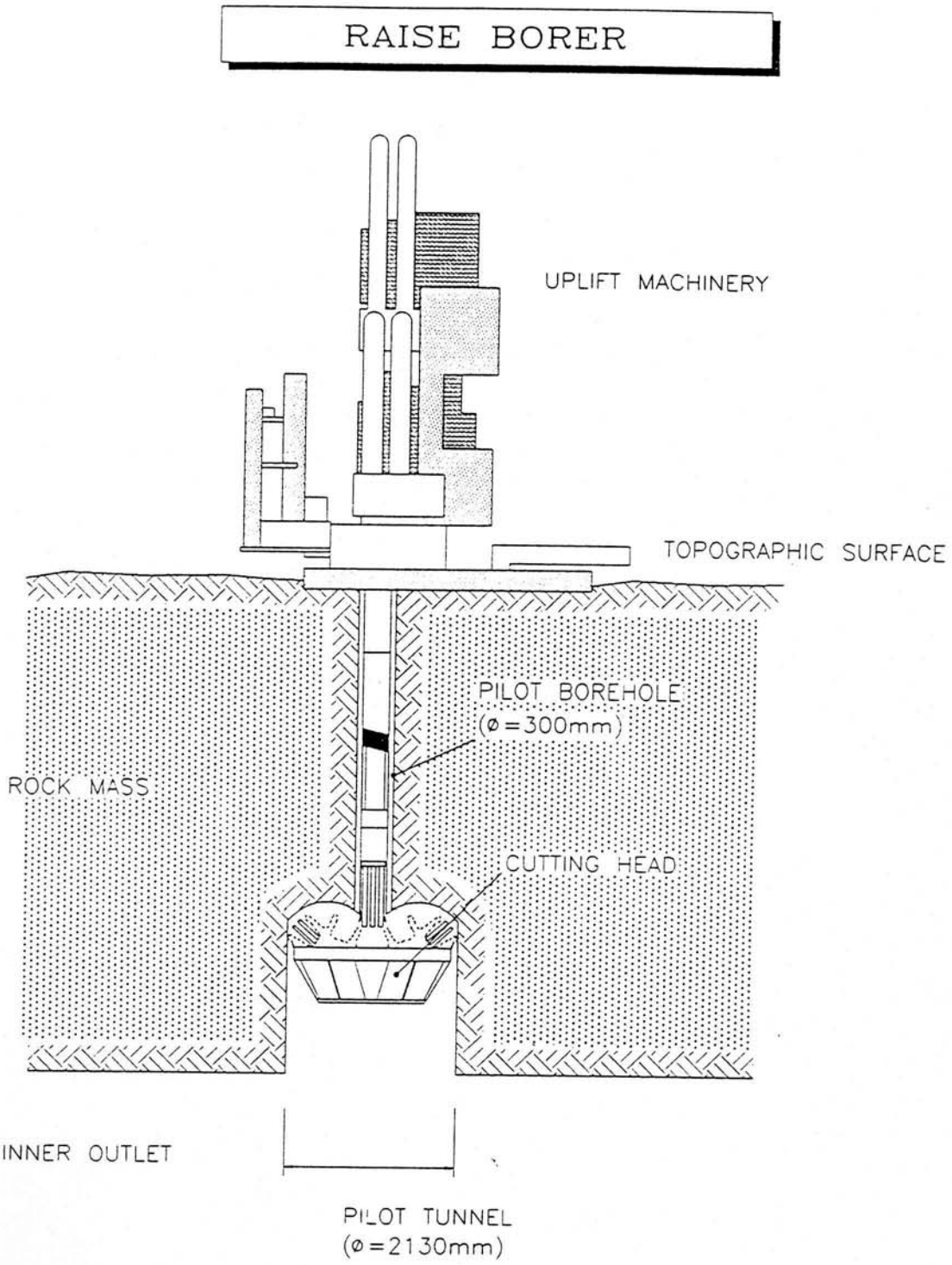

Fig. 4. Schematic view of the raise borer machine.

In the opinion of the authors, the greater compactness is mainly due to greater tightening of the discontinuities rather than to a lower level of fracturing.

GEOPHYSICAL SURVEY

Two tomographic seismic propsections were carried out on each of the slopes adjacent to the dam. The survey was carried out to determine the velocity of the longitudinal seismic waves (P waves) and to find their distribution along horizontal and vertical sections inside the rock mass.

A total of five tomographic surveys were carried out:

—2 on the right side, horizontal and vertical;
—3 on the left side, horizontal, vertical and transverse.

Figure 9 shows the location of the surveys and the position of the sections under examination.

In order to achieve the data for the subvertical sections 48 geophones were used, for each section, on the right side (24 on the left side). They were sited inide the bottom discharge tunnels. A total of 48 explosive charges (24 on the left side) were blasted vertically above on the slopes.

Table 2

Raise borer	Specific energy: Pilot hole ϕ 300 mm	Specific energy: Raise Borer ϕ 2130 mm
Right shaft	74.1 ± 13.72	13.9 ± 2.6 kWh/m³
Inclined right shaft	157.5 ± 38.7	16.9 ± 6.6 kWh/m³
Left shaft	73.8 ± 13.2	18.8 ± 2.5 kWh/m³
Inclined left shaft	219.4 ± 43.7	23.9 ± 4.6 kWh/m³

The same procedure was used to provide the data for the subhorizontal sections, where the geophones were again inside the discharge tunnels while explosions were affected at a horizontal distance at the base of the slopes.

On the right side, the survey was carried out using the "cross shots technique" so as to obtain a large amount of data for statistical analysis. With this technique, the analysis as a whole consisted of $48 \times 24 = 1152$ lines, along which the velocity of the elastic waves was measured. Using this technique, the total amount of data obtained (1152) meant that a very dense grid for investigation resulted.

Special software was used for iterative processing of the data until the best solution was obtained for the system of equations constituted by the trajectories of the seismic rays. Each cell was subject to simultaneous procedures of 20 iterations.

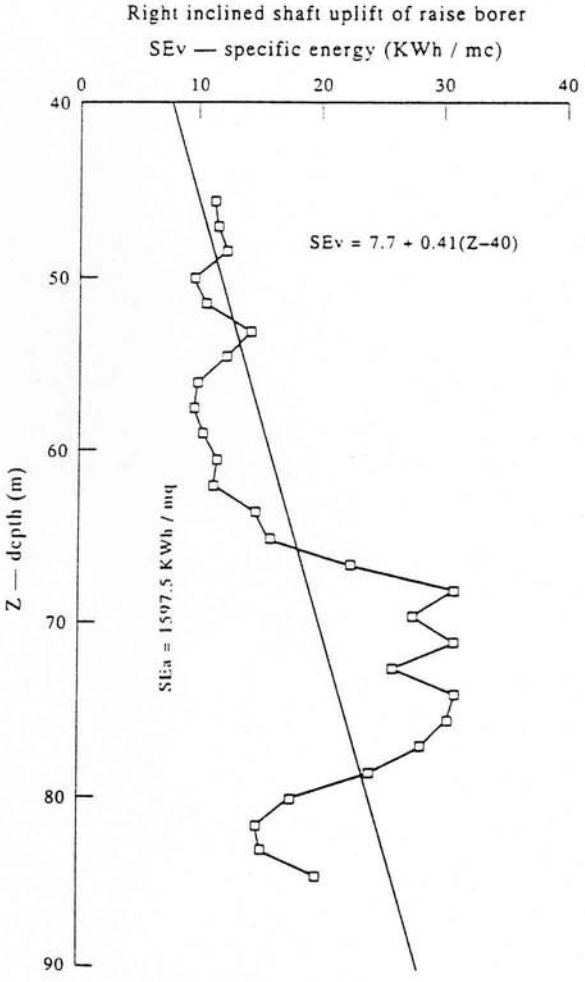

Fig. 5. Diagrams showing logs of SE_v vs depth.

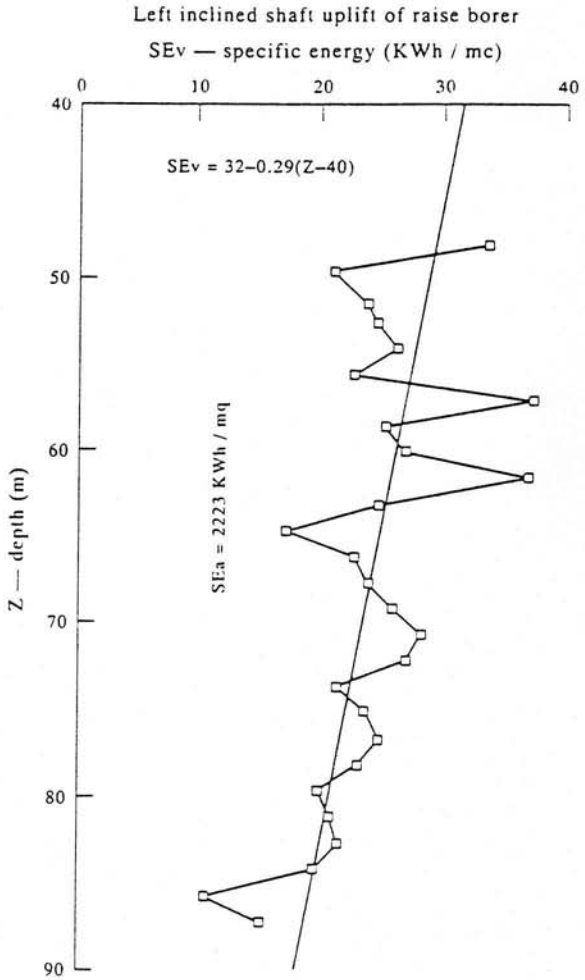

Fig. 6. As for Fig. 5.

Computerized graphic processing of the survey consisted of creating an image where the degree of intensity of the seismic velocities resulting from the composition of the cells analysed was mapped using colour tones proportional to the velocity.

Figure 10 shows the colour tones for 2 of the 5 sections analysed (the vertical and the horizontal of the left abutment).

Analysis of the distribution of the velocities in the individual cells along sections transverse to the valley permitted the construction of topographical sections with lines of equal seismic velocity (velocity contours).

A triangular grid interpolation program (Surfer by Rockware) was used which reconstructed the isolines starting from two seismic lines, one vertical and one horizontal (Fig. 11).

Analysis of the transverse tomographical sections constructed using this method confirmed again the hypotheses concerning the degree of compactness of the rock masses and showed the structure of the fold.

ROCK MECHANICS SURVEY

The purpose of this stage of the survey was to ascertain the strength characteristics of the rock masses. It was felt that *in situ* shear tests on blocks of rock was the best method for ascertaining strength characteristics.

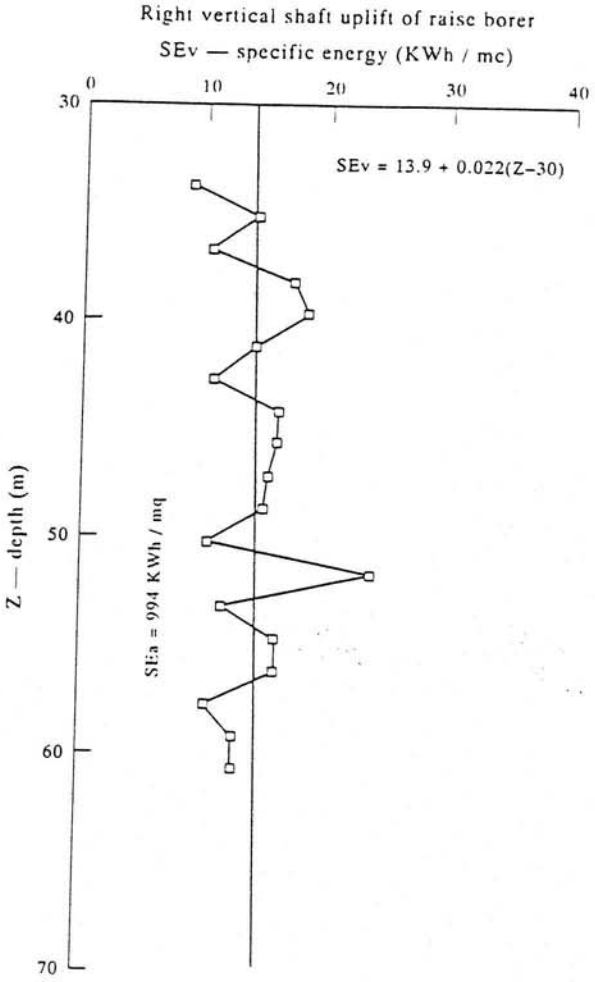

Fig. 7. As for Fig. 5.

The shear tests were carried out on blocks of rock, cubic in shape with the length of one side equal, on average, to approximately 50 cm (Fig. 12). The location of the tests was decided on the basis of operating conditions and the geostructural and geomechanical characteristics of the sites chosen for the surveys (Fig. 2).

The criterion for deciding the number of tests to be carried out was that of obtaining sufficient data for statistical analysis. A total of 10 tests were carried out, 8 on the right side and 2 on the left side. The poorer mechanical properties of the rock on the right side were afforded a greater number of tests.

The equipment used consisted of an upper containment case (box) to house the block and a lower opposing frame. The normal and tangential forces (hydraulic jacks) were transmitted to the block in different ways:

—the normal load is transmitted with a "contrast upper beam" on the containment case (box) connected to tie rods installed laterally to the block, anchored to the ground and positioned perpendicularly to the shear plane;
—the tangential load is transmitted to the upper containment case (box) with horizontal tie rods anchored to the lower contrast frame.

Measurement of the forces applied was effected using precision pressure gauges: displacements of the block parallel and normal to the surface were measured using micrometer-comparators, giving analogue readings (dial gauges). In order to obtain more points from each individual shear test, tests were carried out with three shear cycles bringing the rock close to failure for each value of the normal load. The beginning of the test consisted of a phase of cyclical compression and decompression to recompact the rock loosened by its excavation. After this, the actual test itself was begun. It consisted, for each normal load, of the following phases:

—application of the normal load (and measurement of vertical displacement);
—application at slow velocity of the shear force (with measurement of horizontal displacement);
—interruption of the shear force and release of the normal stress.

The last phase was decided by the operator on the basis of predetermined displacement values (2–3 mm approx.) or when the stress–displacement gradient falls visibly (incipient failure). Following this, another two shear cycles were carried out with two different and increasing values for the normal force. The test finished with three more cycles of increasing normal loads carried out until large displacements were obtained characteristic of a residual shear surface strength.

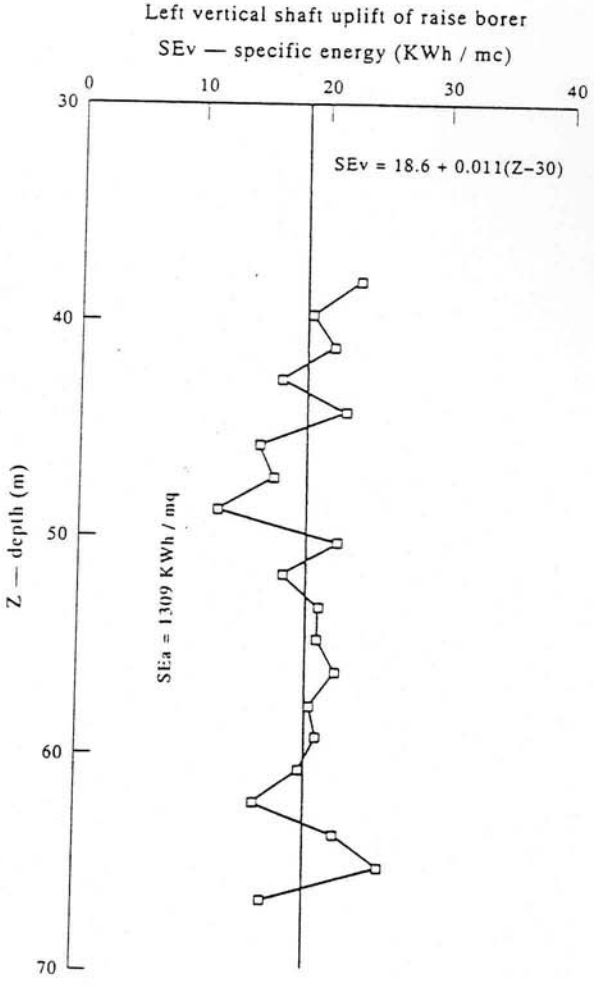

Fig. 8. As for Fig. 5.

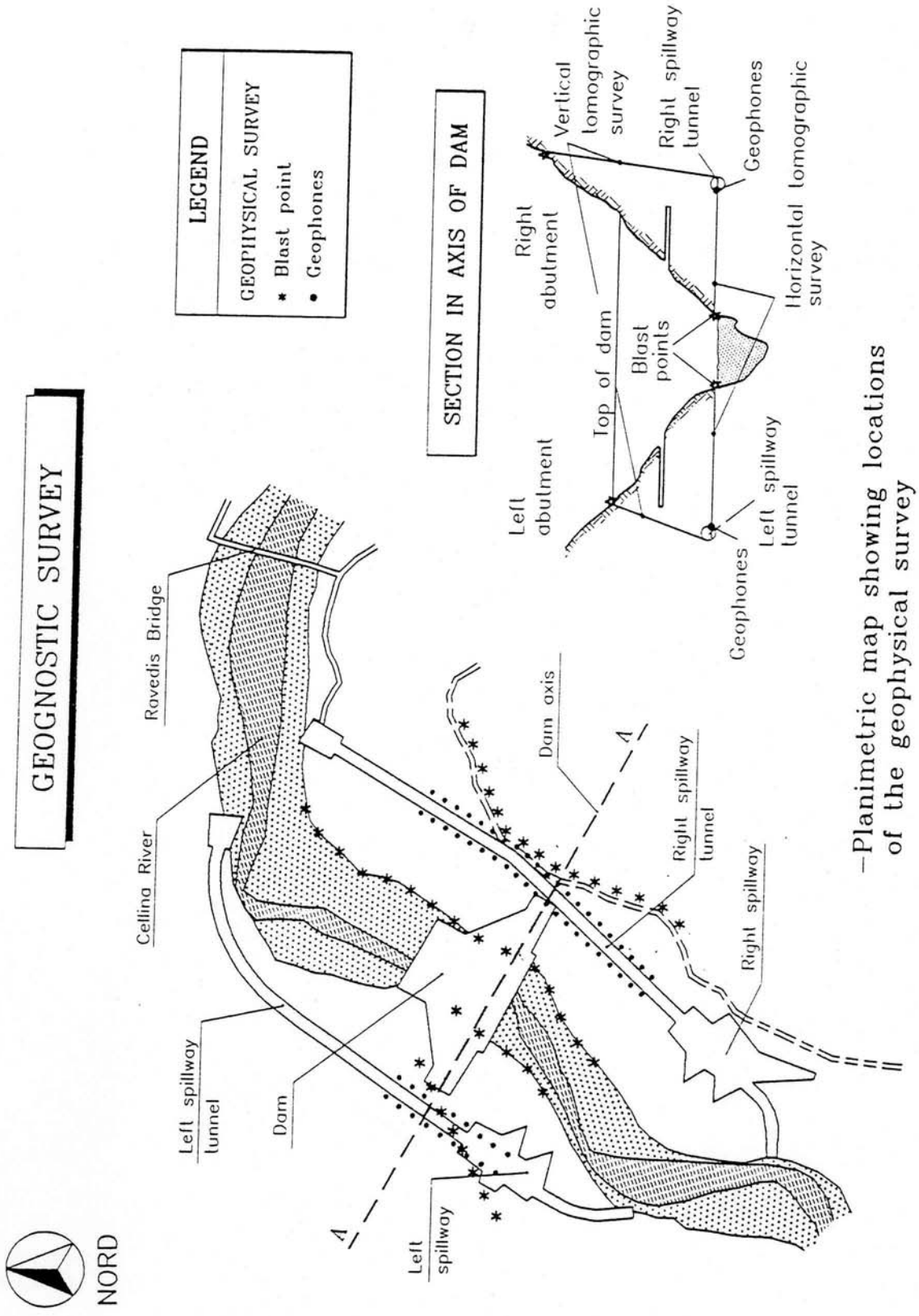

Fig. 9. Map showing location of the single shot points and the receiving geophones in the left and in the right side of the valley.

Tomographic survey
horizontal and vertical sections
of the left abutment

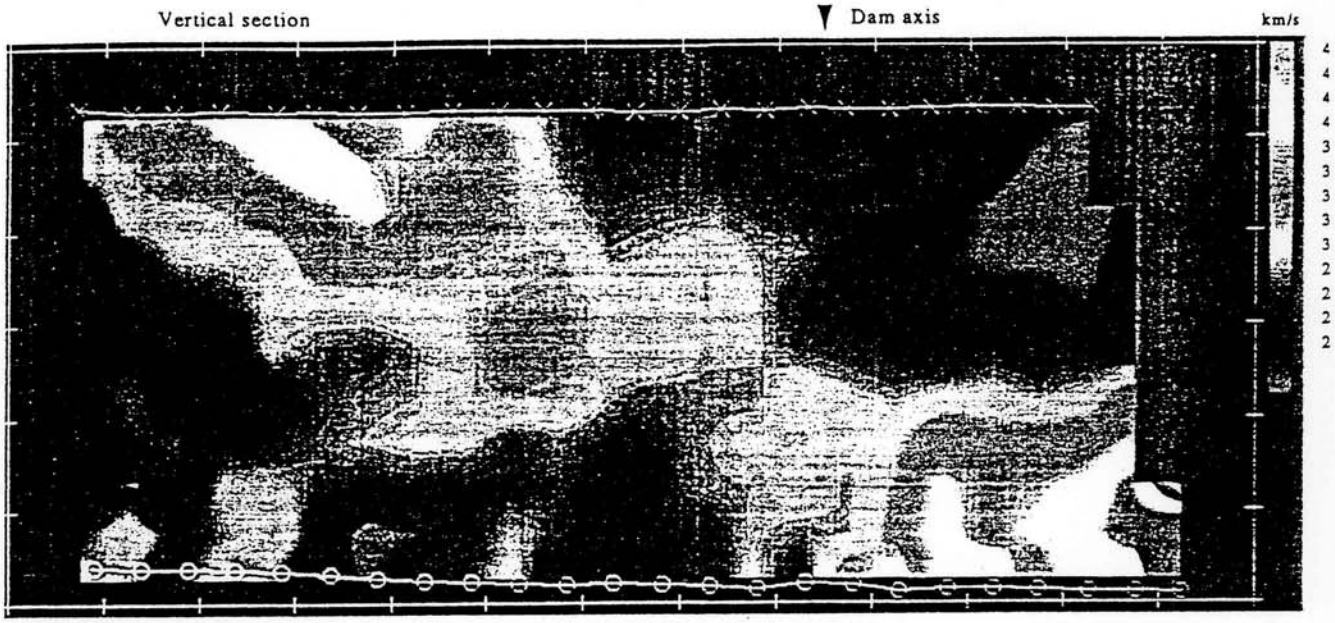

Tomographic analysis of the vertical survey; P — Waves velocities
X = Shot points O = Geophones
Distance between shot points = 10 m

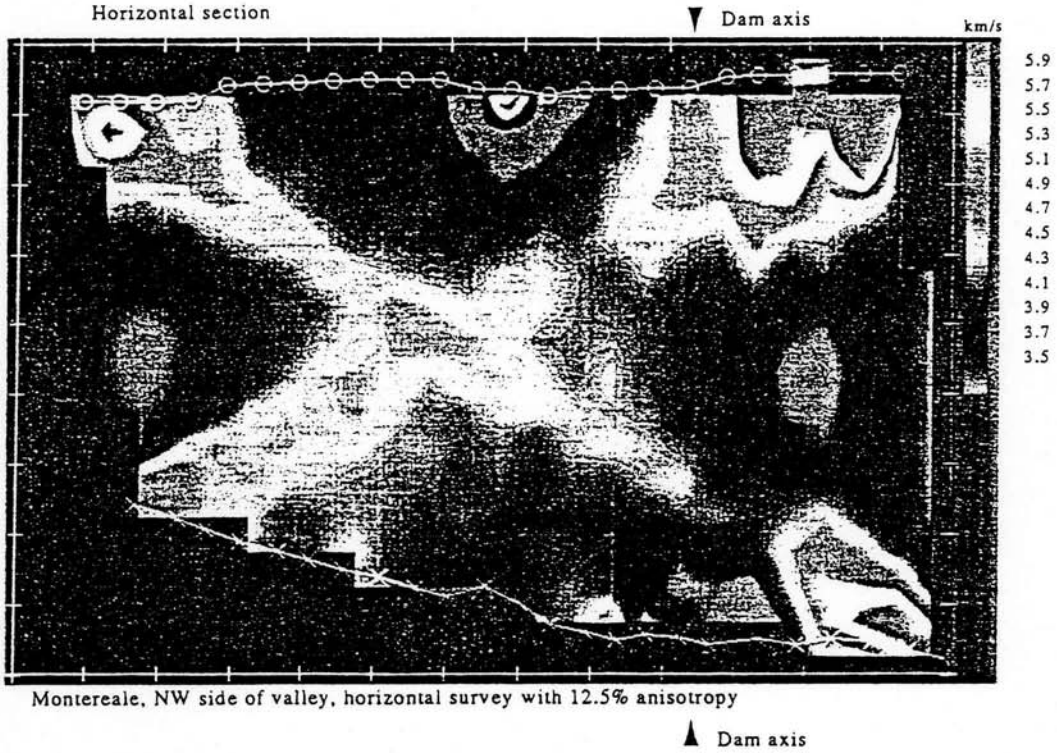

Tomographic analysis of the horizontal survey; P — Waves velocities
X = Shot points O = Geophones
Distance between shot points = 10 m

Fig. 10. Colour maps of the tomographical survey.

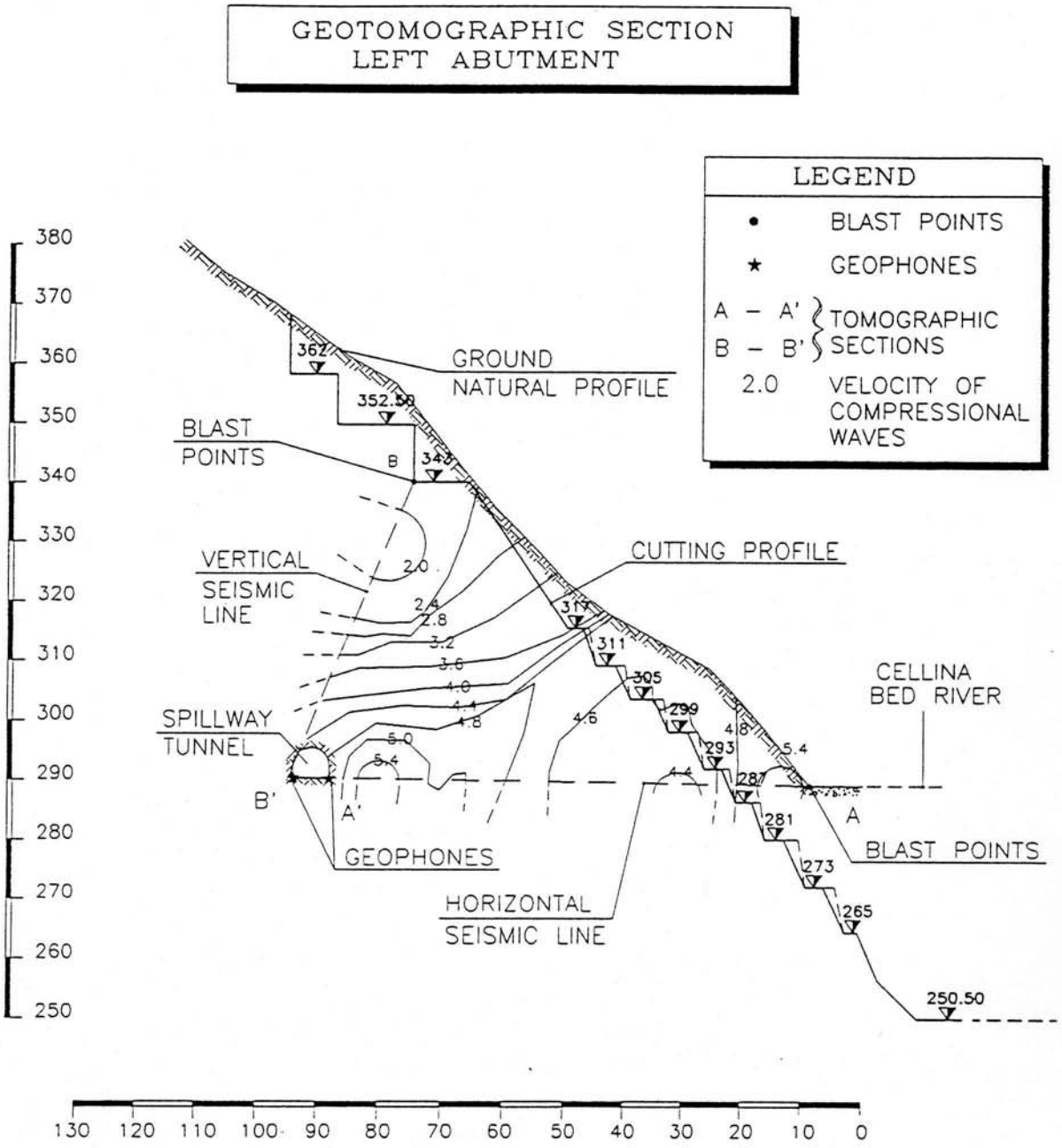

Fig. 11. Tomographical transverse section No. 1 constructed by velocities analysis and interpolation.

On completion of the test, the shear surface was examined and measured. Figure 13 gives a diagram of a block subject to testing, the measurements and observations carried out after the test and its stress–strain behaviour.

The following was measured for each test:

—horizontal and vertical displacements during each phase of shearing;
—pairs of N and T values during each phase of shearing;

The pairs of values N and T were corrected as a function of normal expansion during the tests. This correction was carried out as illustrated in Fig. 14 and consisted of a modification of the values of each individual σ–τ pair as a function of the real expansion developed during the shear cycle. The "expansion" is represented by the angle i which can be considered as the angle of instantaneous inclination of the hypothetical shear surface and is variable during the failure process.

The expansion i (dilatancy) is defined as:

$$i = \arctan(dZ/dX) = \arctan(\delta_n/\delta_t) \quad (3)$$

where

δ_n = normal displacement
δ_t = tangential displacement.

The corrected pairs of σ and τ values are obtained as follows:

$$\sigma' = \sigma * \cos i + \tau * \sin i \quad (4)$$

$$\tau' = \tau * \cos i + \sigma * \sin i \quad (5)$$

The authors felt that it was important to carry out the corrections for expansion to find the real net strength

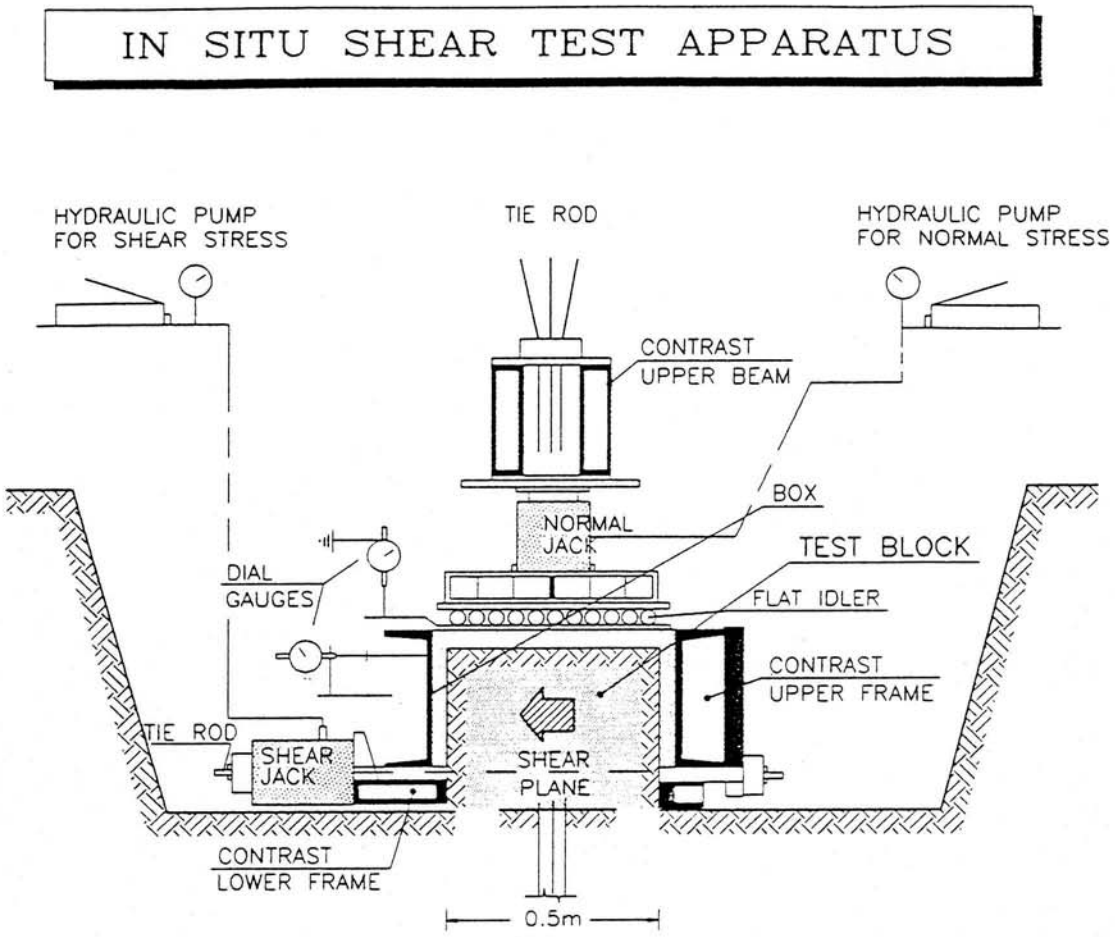

Fig. 12. Schematic view of the shear test *in situ* apparatus.

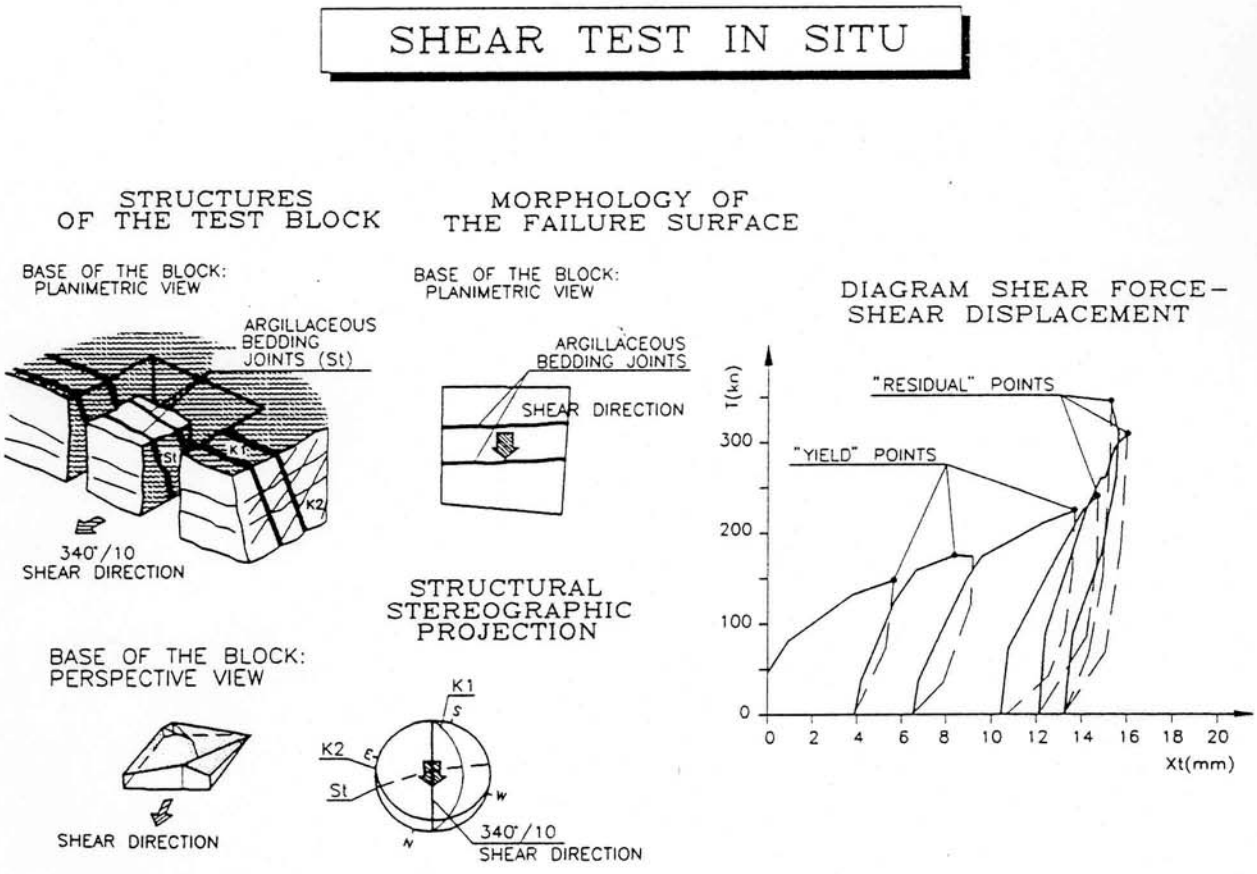

Fig. 13. Schematic view of the block survey and diagram showing block behaviour during the test.

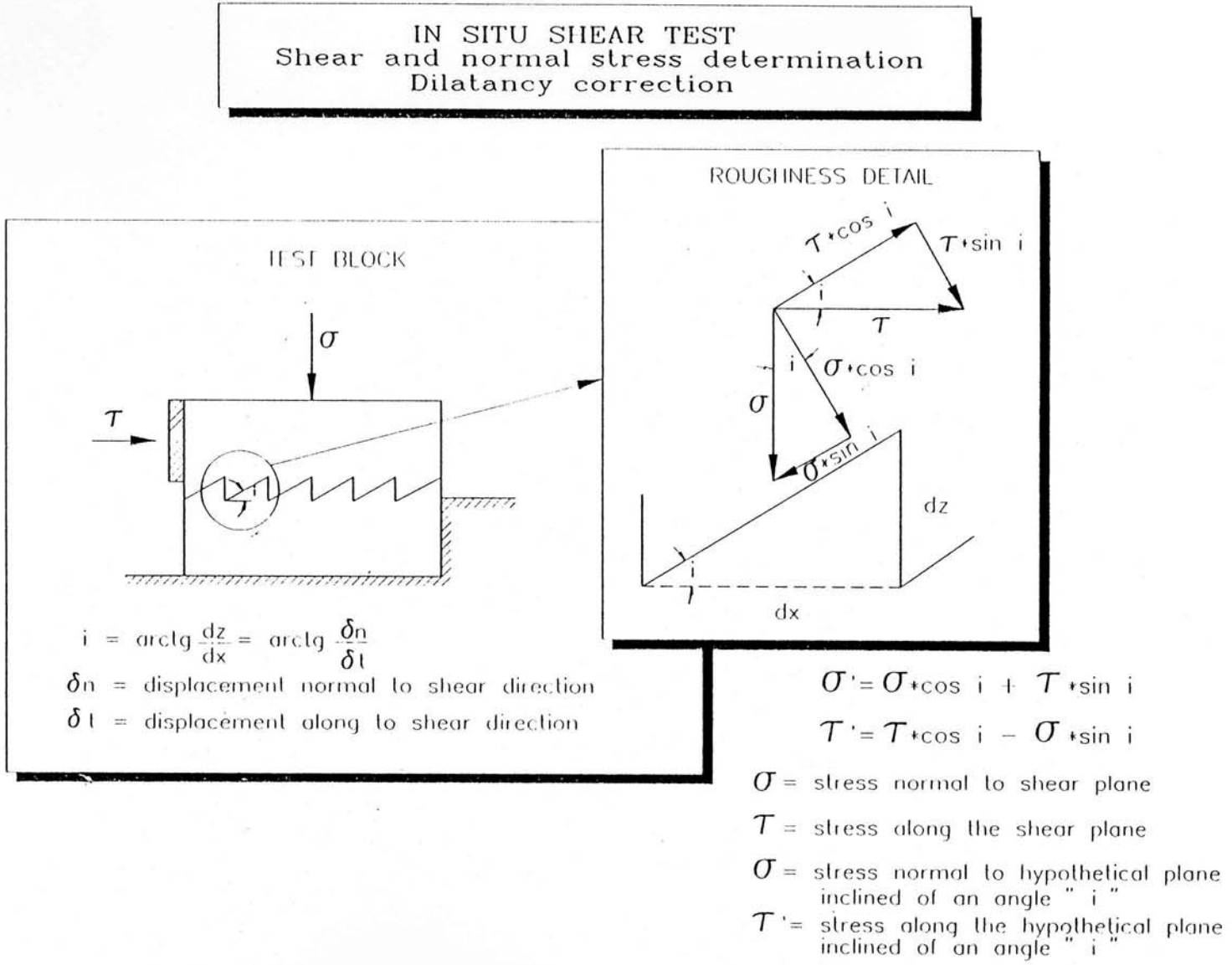

Fig. 14. Scheme of the "dilatancy correction" taking into account the expansion during the test.

values after stresses that do not develop along the set shear plane are subtracted.

The value i was obtained using two different methods according to the block under test:

—by measuring the δ_n/δ_t gradient during the test;
—by measuring the inclination of the failure plane from the horizontal.

ROCK MASS STRENGTH

In order to obtain the stress diagram of the materials, the shear test data were processed in accordance with the Hoek and Brown strength criterion [2]. This criterion expressed in terms of principal stresses is defined by the following expression:

$$\sigma_1 = \sigma_3 + (m * \sigma_c * \sigma_3 + s * \sigma_c^2)^{0.5} \quad (6)$$

where

σ_1 = maximum principal stress at the failure
σ_3 = minimum principal stress at the failure
σ_c = uniaxial compressive strength of the intact material (rock material)
m,s = experimentally determined empirical constants.

In order to determine the value for σ_c, which defines the failure strength of the intact material, uniaxial tests were carried out in the laboratory and these provided an average value of $\sigma_c = 50$ MPa. The parameters m and s were obtained following Hoek and Brown [3] converting the values σ' and τ' into σ_1 and σ_3. The operation was carried out by fixing a cohesion value c obtained by linear regression (best fit) of the points σ' and τ' [3].

Table 3 gives the values for m and s for all the tests carried out and the values C and ϕ obtained using linear regression. The same table also gives the values of σ_{gd} (σ geotechnical design) which is to say the compressive strength values of the rock mass ($\sigma_{gd} = (s * \sigma_c^2)^{0.5}$).

The strength diagrams for the individual blocks of rock (Fig. 15) were obtained from the values m and s. These strength diagrams were compared with those obtained during the preliminary studies (Fig. 16). The latter were obtained using the Bieniawski classification [4] and by applying the formulas of Priest and Brown [5] for the calculation of the values m and s for the rock mass.

The Priest and Brown formulas state the following for disturbed rock masses:

$$m = \exp\left(\frac{\mathrm{RMR} - 100}{14}\right) \cdot m_i \quad (7)$$

$$s = \exp\left(\frac{\mathrm{RMR} - 100}{6}\right) \quad (8)$$

where

m_i = empirical constant for intact material
RMR = rock mass rating of Bieniawski.

Barton's strength criterion [6] was used for the joints.

Table 3

Test No.	Site	Structure	Best-fit (Mohr–Coulomb)	Hoek and Brown (σ_c = 50 MPa)	σ_{gd} (MPa)
1	Right spillway	Joint	c = 0.5 MPa ϕ = 23° r = 0.96	m = 0.098856 s = 0.001156	1.7
2	Right spillway	Rock mass	c = 0.2 MPa ϕ = 23° r = 0.997	m = 1.277722 s = 0	0
3	Right spillway	Rock mass	c = 0.2 MPa ϕ = 23° r = 0.95	m = 0.0655 s = 0.000115	0.54
4	Right spillway	Filled joint	c = 0.4 MPa ϕ = 11° r = 1.00	m = 0.0205 s = 0.000477	1.19
5	Right spillway	Joint	c = 0.4 MPa ϕ = 43° r = 0.97	m = 0.557503 s = 0.00057	1.19
6	Right spillway	Joint	c = 0.5 MPa ϕ = 41° r = 0.98	m = 0.498862 s = 0.001244	1.76
7	Right abutment	Rock mass	c = 0.4 MPa ϕ = 47° r = 0.97	m = 0.861667 s = 0.001531	1.96
8	Right abutment	Rock mass	c = 0.4 MPa ϕ = 43° r = 0.98	m = 0.468337 s = 0.001908	2.18
9	Left abutment	Rock mass	c = 0.5 MPa ϕ = 28° r = 0.999	m = 0.143094 s = 0.001572	1.98
10	Left spillway	Rock mass	c = 0.05 MPa ϕ = 55° r = 0.99	m = 1.1747826 s = 0	0

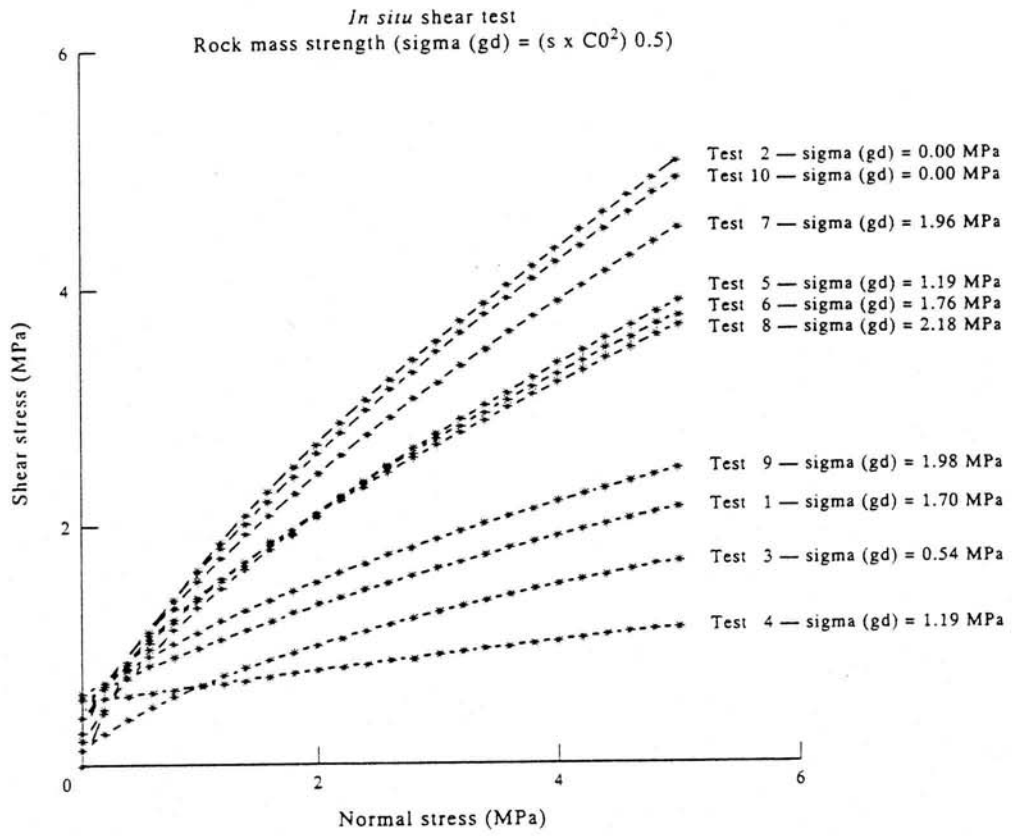

Fig. 15. Diagrams of the shear rock masses strength from tests *in situ* by Hoek and Brown strength criterion processing.

Barton's strength criterion states:

$$\tau_{mob} = \sigma_n \cdot \phi_{mob} \tag{9}$$

where

$$\phi_{mob} = \text{available friction angle} = \\ = \phi_b + \text{JRC} * \log(\text{JCS}/\sigma_n) \tag{10}$$

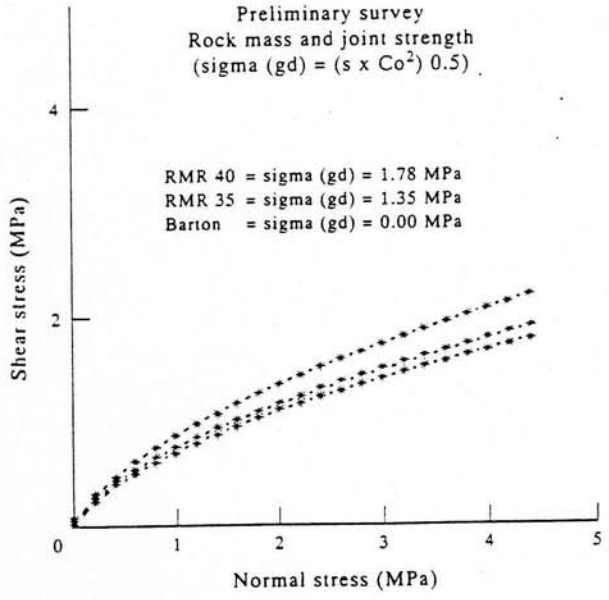

Fig. 16. Diagrams of the rock masses and joint shear strength from Bieniawski classification and Barton theory and using Hoek and Brown and Barton strength criteria for processing data.

where

ϕ_b = base friction angle
JRC = joint roughness coefficient
JCS = joint compressive strength.

A comparison of the estimated stress diagrams with those obtained experimentally showed close correspondence only for the lowest class of the experimental diagrams. The estimates turned out to be quite conservative.

ROCK SLOPE STABILITY ANALYSIS

It was necessary to calculate the safety coefficient of excavated and natural slopes in order to comply with the requirements of the Ministerial Decrees relating to Governmental Technical Authorities (Dams Service). These Rules in Law require safety coefficients for excavation of equal to or greater than 1.3.

No precise numerical value is required for natural slopes overlooking dams: for these the design engineering geologists must decide on a reference value based on his/her knowledge of the problem The authors adopted a minimum safety coefficient of 1.3.

Stability analysis was carried out on 12 representative sections. Section 1 (left side) is given as an example (Fig. 17).

The authors felt that it was important to make some changes to the calculations carried out by the computer software (Bell method) [1] in order to:

(a) take into account a non-linear type strength criterion for the rock mass (Hoek and Brown);

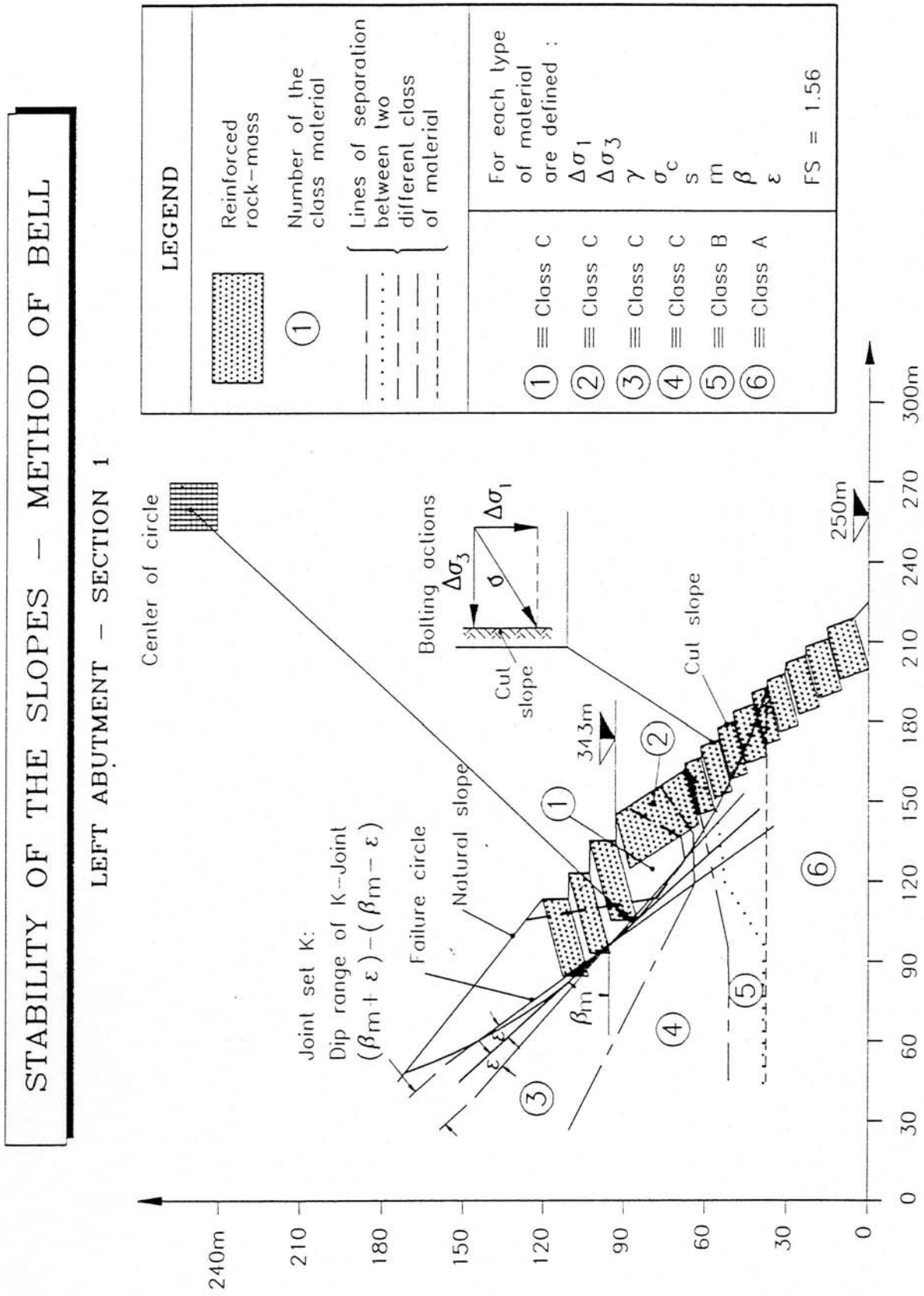

Fig. 17. Scheme of the changes improved on the method of Bell.

(b) take into account the presence of geological discontinuities in the rock mass;
(c) take into account reinforcement interventions by enhancing the strength characteristics of the rock mass.

Bell's equilibrium limit method, carried out using a computer for the calculations, was modified in accordance with points (a), (b) and (c). Classification of the materials of the section subject to analysis necessary for the application of the Bell method was carried out using data from the geophysical survey and from the *in situ* shear tests.

The analysis of the geotomographical survey, which furnished geoseismic sections with contours of seismic velocity, was used for attributing different strength values to the differing density values obtained.

Three classes of rock masses were identified, from the data obtained from the geophysical survey, as a function of the velocity of the seismic waves (V_p);

class A = $V_p > 4.0$ km/sec
class B = 3.5 km/sec $< V_p < 4.0$ km/sec
class C = $V_p < 3.5$ km/sec.

The authors felt that the degree of compactness of the rock mass (density) should correlate with its strength properties.

Three representative stress diagrams were attributed to the three classes A, B and C (Fig. 15):

class A = diagram 7
class B = diagram 8
class C = diagram 1.

Figure 15 shows that the diagrams chosen to represent the strength classes fall within three bands of distinct diagrams. The following were chosen for discontinuity strength characteristics:

discontinuity without plastic filling = diagram 3
discontinuity with plastic filling = diagram 4.

The original calculation procedure defined by Bell had to be changed for point (a). The Bell method (Fig. 18) resolves the static uncertainty of the problem by formulating a hypothesis for the distribution of normal stresses along the line of slip.

According to the Bell method:

$$\sigma_n = C1 * (1 - K_y) * (W_i * \cos A_i)/L_i + C2 * \sin 360^\circ * (X_b - X_i)/(X_b - X_a) \quad (11)$$

where the symbols K_y, W_i, A_i, L_i, X_b, X_a and X_i are shown in Fig. 18 and $C1$ and $C2$ are the unknowns of the problem together with FS = factor of safety.

These unknowns are obtained *a posteriori* after Bell's equilibrium system has been resolved. A method of approximates was used for the attribution of the parameters C and ϕ, which in the Hoek and Brown criterion depend on the parameter σ_n.

With the modified computer program, the following operations are carried out:

(1) calculation of the values for σ_n on the base of the slices according to a lithostatic criterion;
(2) calculation of the values for C_i and ϕ_i (instantaneous) of the strength diagram for each individual segment according to Hoek and Brown's equation;
(3) execution of the Bell method.

The use of this system was checked by comparing the stress distribution (normal stress) on the base of the slices, as calculated according to Bell, with those hypothesized for the resolution of the problem (lithostatic stress), inside the same section (Fig. 17). The modified calculation method can be considered valid as it results in stress distributions along the slip line according to Bell similar to those obtained using a lithostatic criteria (Fig. 19).

The modified procedure tends, during the phase for the calculation of C_i and ϕ_i, to overestimate the level of normal stress σ_n used subsequently for resolving the system of unknowns. In the case in question, this effect is particularly visible in one particular zone of the slip line. Here the Hoek and Brown instantaneous cohesion values are greater than would be required by the σ_n of Bell and are attributed to the rock.

The insertion of problem (b) into the computer code was simply achieved. It was considered that the inclination (β) of the discontinuity surfaces K falls statistically within a range of values (Fig. 17) defined by:

$$\beta_m + \epsilon > \beta > \beta_m - \epsilon$$

(according to a Gaussian probability curve) (12)

where

β = inclination of the discontinuity surface K
β_m = average inclination of the set of discontinuity surfaces K
ϵ = standard deviation of the inclination of the set of discontinuities K.

A modification was introduced to the computer code so as to be able to use the strength characteristics of the discontinuities when A_i (inclination of the base of segment i) falls within the range defined above, which is to say when:

$$\beta_m + \epsilon > A_i > \beta_m - \epsilon. \quad (13)$$

This means that failure can be considered as occurring locally along existing discontinuity surfaces when the slip surface is close to those discontinuities.

In order to solve problem (c) further modifications were made to the computer program.

The reinforcement of excavated slopes was dealt with; this consisted of high strength steel bolts fully grouted and stressed. In the opinion of the authors, for reasons of safety, the best method for taking into account the effect of reinforcement is to increase the shear strength properties of the rock mass, as is generally done in the case of fully grouted passive bolts [7–9]. With this

METHOD OF BELL

LIMIT EQUILIBRIUM WITH VERTICAL SLICES

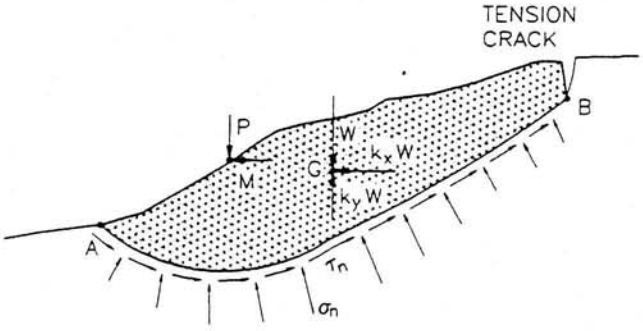

DEFINITION OF THE LIMIT EQUILIBRIUM PROBLEM OF THE SLIDING MASS.

LEGEND

W	=	WEIGHT OF THE SLICE
$k_x W_i$, $k_y W_i$	=	SEISMIC FORCES
Q, P	=	HORIZONTAL & VERTICAL COMPONENTS OF THE RESULTANT OF THE EXTERNAL LOADS, IN THE POINT M (X_M, Y_M)
N_i, T_i	=	NORMAL AND SHEAR FORCES ON THE BASE OF THE SLICE

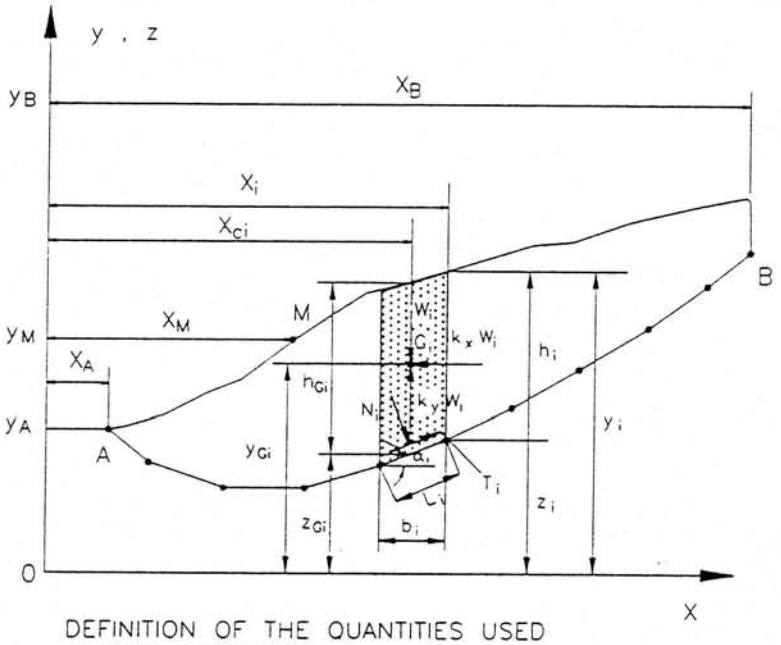

DEFINITION OF THE QUANTITIES USED IN THE CALCULUS.

Fig. 18. Static scheme of the slices equilibrium method of Bell.

method, the reinforcing effect is considered by means of an increase in cohesion, which is to say an increase in resistant forces known as cohesive reinforcement [10]. The zone affected by the reinforcement treatment can be defined geometrically with this method and it is more suitable for the application of an external force (Fig. 17).

Several studies have been carried out to simulate the increase in cohesion that occurs in rock reinforced with metallic bolts. Egger [11] carried out an initial analysis of the problem and proposed a formula for an increment in cohesion, dependent on the pure shear effect alone offered by the reinforcement bolt. The cohesion increment provided by the reinforcement (C_b) is:

$$C_b = 0.6 * \frac{\pi * d_b^2}{4 * s^2} * \sigma_s \left[\frac{\sigma_c}{\sigma_s}\right]^{0.5} \qquad (14)$$

where

d_b = diameter of the bolt
s = side of anchor network
σ_c = yield stress of the bolt
σ_s = uniaxial compressive strength of the rock.

The approach used by the authors consisted of quantifying the increment in strength of the rock mass, as reinforced by the steel bolt, by considering the tensile shear effect and the pure shear effect.

The concept assumes the presence of fully grouted bolts with passive type functioning.

With this approach, the tensile shear effect is calculated [12] by using the Coulomb strength criterion expressed in terms of principal stresses (σ_1, σ_3) from which:

$$\sigma_1 = 2 * C * \tan(45° + \phi/2) + \tan^2(45° + \phi/2) * \sigma_3 \quad (15)$$

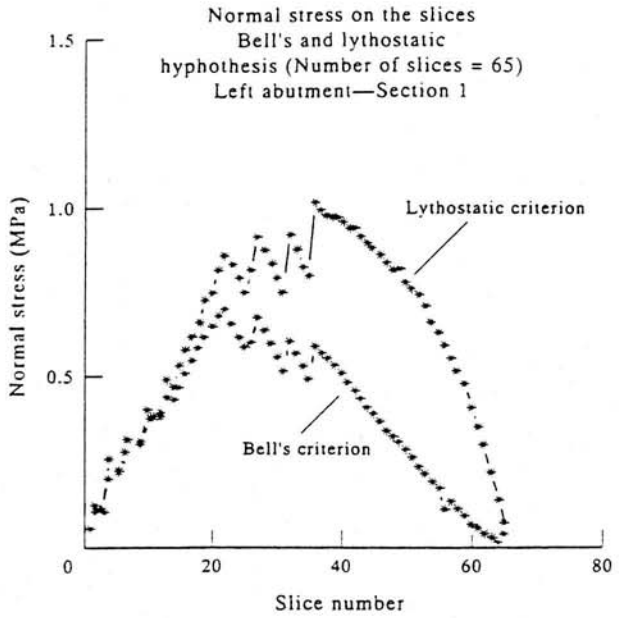

Fig. 19. Diagrams showing the gap between the σ_n values by using lithostatic and Bell criteria.

where

C = cohesion of the rock mass
ϕ = friction angle of the rock mass.

If the influence of the reinforcement in the rock is summed in equation (14), the following is obtained:

$$\sigma_1'' = 2 * C'' * \tan(45° + \phi/2) + \tan^2(45° + \phi/2) * \sigma_3 \quad (16)$$

where

σ_1'' = principal incremented maximum stress
C'' = incremented cohesion of the rock mass.

The term C'' is expressed as:

$$C'' = C + [\Delta\sigma_3 * \tan(45° + \phi/2)] * 0.5 \quad (17)$$

where

$\Delta\sigma_3$ = horizontal component of the force of the bolts.

Method (12) was introduced into the computer program and represents the tensile shear strength effect of the rock and grouted bolt as a single entity.

According to the diagram in Fig. 18 the base of each slice can be considered as being subject to a normal force and a tangential force. The strength of the base of an individual slice can be calculated in the following stages:

(1) calculation of σ_n on the base of the slice
(2) calculation of the Hoek and Brown values C_i and ϕ_i on the base of the slice
(3) calculation of $\Delta\sigma_3$ (horizontal component of the force of the bolts)
(4) calculation of $\Delta\sigma_1$ (vertical component of the force of the bolts) and its breakdown into σ_n and τ on the base of the slice
(5) calculation of the value C'' for each slice
(6) execution of the Bell method.

This calculation method was very fast due to the simplicity of the variation in the parameters.

In order to represent the pure shear strength offered by the bolt (Fig. 20) a further increment to the strength of the rock mass was effected, this being due to the "Dowel effect" [13].

In the opinion of the author who has studied it (Bjurstrom, [13]), this effect (T_d) depends on three parameters of the bolt–grout unit.

(1) The diameter of the bolt (d_b)
(2) Uniaxial compressive strength of the cement grouting material in the hole (σ_c)
(3) Yield stress of the bolt (σ_s)

The contribution of the shear strength of each individual bolt can be summarized by the equation:

$$T_d = d_b^2 * 0.67 * (\sigma_s * \sigma_c)^{0.5}[\text{MPa}] \quad (18)$$

where the parameters are expressed in:

d_b [m]
σ_s [MPa]
σ_c [MPa]

In terms of the increase in cohesion (C_d = cohesion due to the "Dowel effect") the following can be stated:

$$C_d = (n * T_d)/s \quad (19)$$

where

n = the number of bolts that intersect the slip surface
s = development of the slip surface.

This cohesion increment effect was inserted in the computer program, considering the parameters n_i and s_i for the base of each slice.

$n_i = (L_i * \sin A_i)/S_i$ = the number of bolts that intersect the base of the ith slice (20)
$s_i = L_i$ = the areal development of the ith slice
a_i = the area of influence of each bolt on a vertical face of excavation (= vertical distance between centres of bolts).

Finally summing the increment in cohesion for tensile shear (C'') and that for pure shear (C_d) to the natural cohesion of the rock mass (C_{RM}), the cohesion value for the reinforced rock mass (C_{RRM}) is obtained:

$$C_{RRM} = C_{RM} + C'' + C_d \quad (21)$$

CONCLUSION

The need to define safety coefficients (factors of safety) for the rock excavations and natural slopes of the Ravedis Dam led to the use of simple and repeatable stability analysis. The choice of calculation method fell on the slices equilibrium method of general application in soil mechanics (Bell method).

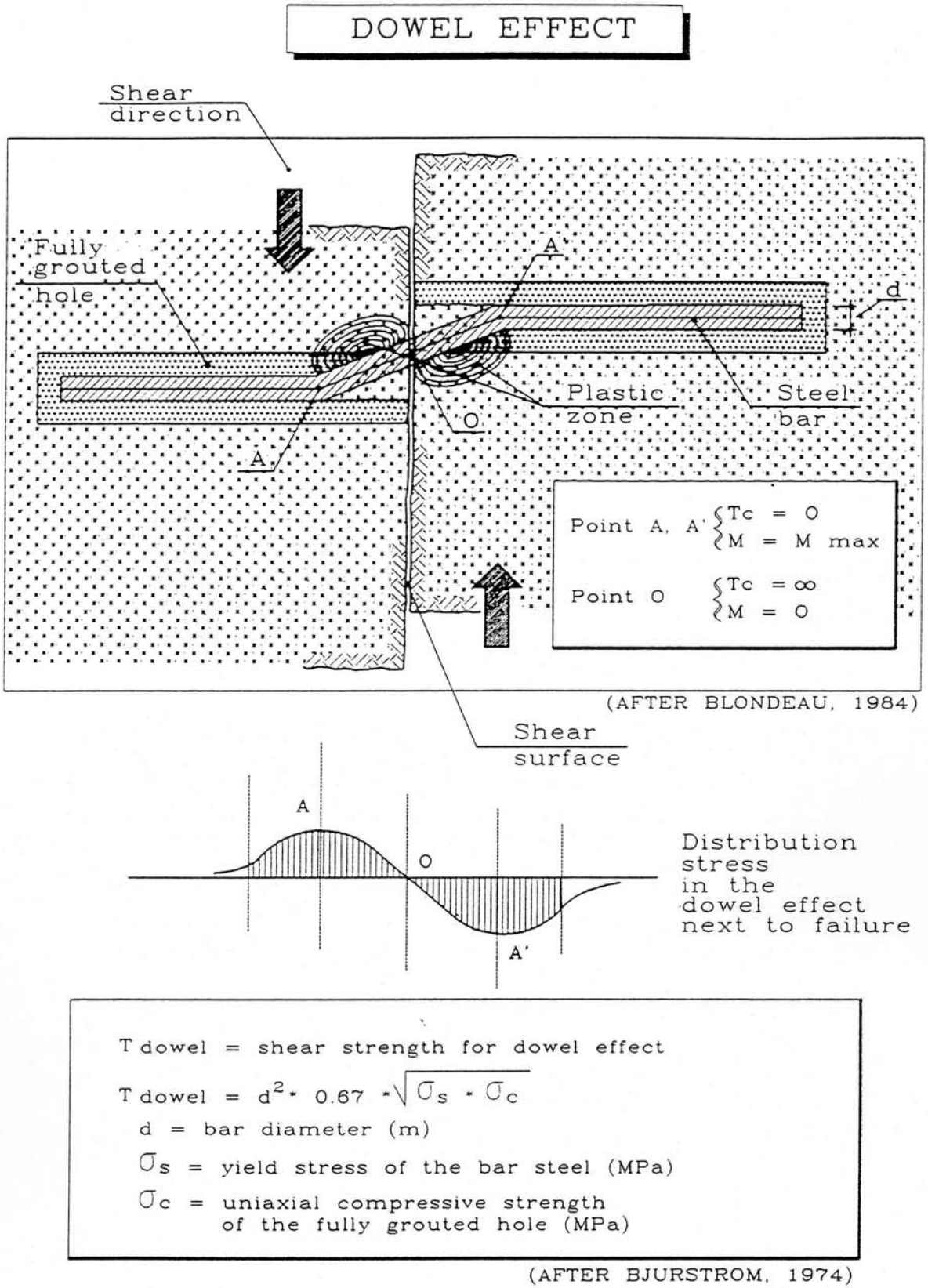

Fig. 20. Static scheme and pictorial view of the "Dowel effect".

Some modifications were made to this method in order to be able to use it for the study of rock slope stability. These modifications made it possible to:

—use a non-linear strength criterion;
—take into account geological discontinuities;
—take into account reinforcement as an increment in the strength of the rock mass.

Geostructural, geophysical and geomechanical investigations furnished data on the structure, density and strength of the rock masses and confirmed the geostructural model of the site of the dam.

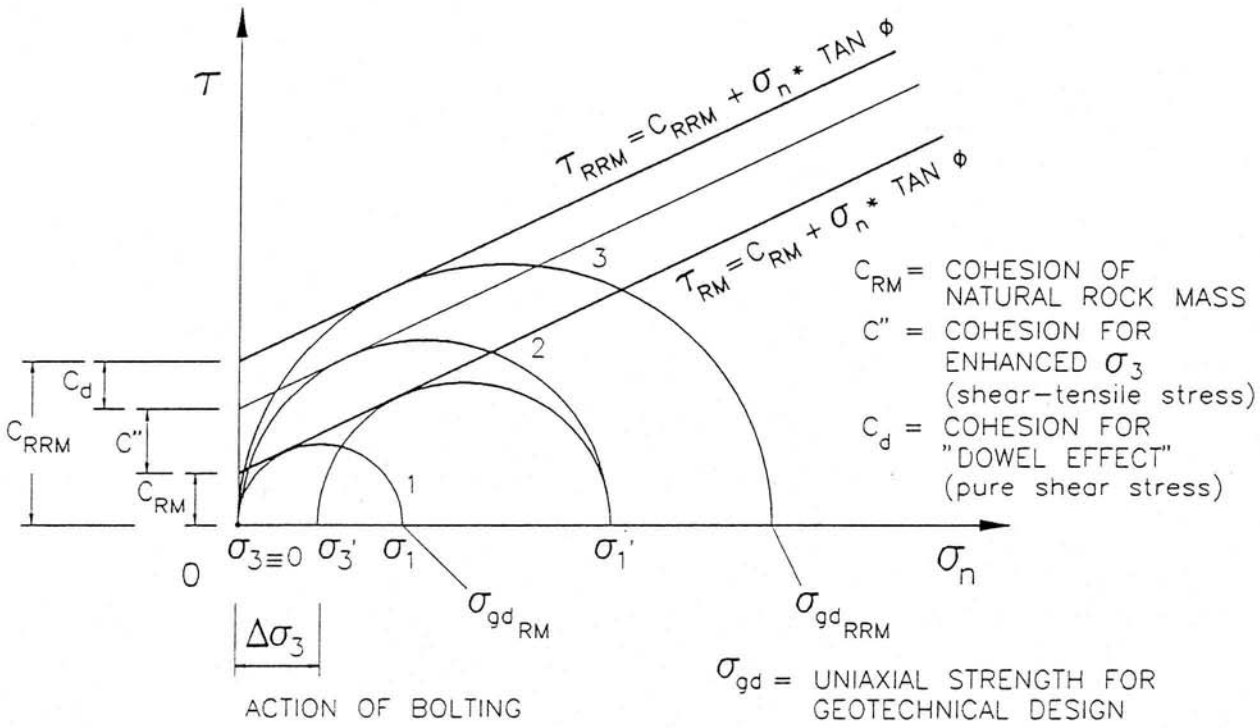

Fig. 21. Scheme resuming enhanced strength rock mass characteristics by bolting.

The calculation method used was found to be suitable and reliable for intensive and repetitive use, as shown by the case in question.

Accepted for publication 7 October 1993.

REFERENCES

1. Bell J. M. General slope stability analysis. *J. Soil Mech. Foundations Div.* **94** (SM6). 1253–1270 (1968).
2. Hoek E. and Brown E. T. Empirical strength criterion for rock masses. *J. Geotech. Engng. Div. Am. Soc. Civ. Engrs* **106**, 1013–1035 (1980).
3. Hoek E. Strength of jointed rock masses. *Geotechnique* **33**, 187–223 (1983).
4. Bieniawski Z. T. Geomechanics classification of rock masses and its applications in tunnelling. *Proc. 3rd Int. Congr. on Rock Mech.* Denver 2, Part A, pp. 27–32 (1972).
5. Priest S. D. and Brown E. T. Probabilistic stability analysis of variable rock slopes. *Trans. Inst. Min. Metall.* **92**, A1–A12 (1983).
6. Barton N. Review of a new shear-strength criterion for rock joints. *Engng Geol.* 7, 287–332 (1973).
7. Panet M. Stabilization et reinforcement des massifs rocheux par aciers précontraints et aciers passifs. Atti del Seminario sul consolidamento di terreni e rocce in posto nell'ingegneria civile. *Stresa* 33–62 (1978).
8. Azuar M. M., Debreville, Habib, Londe, Panet, Rochet, Salem-Bier. Le reinforcement des massifs rocheux par armatu res passives. *Proc. 4th ISRM Cong.* Montreux, Vol. 1, pp. 23–29 (1979).
9. Panet M. Ground reinforcement by bolts in tunnelling. *Proc. Il Consolidamento del Suolo e delle Rocce Nelle Realizzazioni in Sotterraneo*, Vol. 1, pp. 31–41 (1991).
10. Hantz D. Reinforcement de joints rocheux par armature passive. *Nancy—Discontinuum Modeling of Jointed Rock Masses* (1990).
11. Egger P. Nene Gesichtspunkte bei Tunnelankerungen Grundlangen and Anwendung der Felsmechanik. *Felsmechanik kolloquium Kalsruhe*, pp. 263–276. Trans. Tech. Publications (1978).
12. Grasso P. *et al.* The role of cable bolting in ground reinforcement. *Proc. Il Consolidamento del Suolo e delle Rocce Nelle Realizzazioni in Sotterraneo*, pp. 127–138 (1991).
13. Bjurstrom S. Shear strength of hard rock joints reinforced by ground untensioned bolts. *Proc. 3rd Cong. ISRM*, Denver, Vol. 2B, pp. 1194–1199 (1974).